

Mosaic of Somatic Mutations in Earth's Oldest Living Organism, Pando

Rozenn M. Pineau^{a,b,1}, Karen E. Mock^{c,d}, Jesse Morris^e, Vachel Kraklow^f, Andrea Brunelle^e, Aurore Pageot^f, William C. Ratcliff^a, and Zachariah Gompert^{g, 1}

This manuscript was compiled on October 23, 2024

Understanding how mutations arise and spread through individuals and populations is fundamental to evolutionary biology. Most organisms have a life cycle with unicellular bottlenecks during reproduction. However, some organisms like plants, fungi, or colonial animals can grow indefinitely, changing the manner in which mutations spread throughout both the individual and the population. Furthermore, clonally reproducing organisms may also achieve exceedingly long lifespans, making somatic mutation an important mechanism of creating heritable variation for Darwinian evolution by natural selection. Yet, little is known about intra-organism mutation rates and evolutionary trajectories in long-lived species. Here, we study the Pando aspen clone, the largest known quaking aspen (*Populus tremuloides*) clone founded by a single seedling and thought to be one of the oldest studied organisms. Aspen reproduce vegetatively via new root-borne stems forming clonal patches, sometimes spanning several hectares. To study the evolutionary history of the Pando clone, we collected and sequenced over 500 samples from Pando and neighboring clones, as well as from various tissue types within Pando, including leaves, roots, and bark. We applied a series of filters to distinguish somatic mutations from the pool of both somatic and germline mutations, incorporating a technical replicate sequencing approach to account for uncertainty in somatic mutation detection. Despite root spreading being spatially constrained, we observed only a modest positive correlation between genetic and spatial distance, suggesting the presence of a mechanism preventing the accumulation and spread of mutations across units. Phylogenetic models estimate the age of the clone to be between ~16,000-80,000 years. This age is generally corroborated by the near-continuous presence of aspen pollen in a lake sediment record collected from Fish Lake near Pando. Overall, this work enhances understanding of mutation accumulation and dispersal within and between ramets of long-lived, clonally-reproducing organisms.

somatic mutations | clonal organisms | aspen | [other keywords?](#) 5 max

Understanding how mutations arise and spread through a population is essential to understanding biological evolution. The advent of high-throughput genome sequencing has allowed us to study mutational dynamics in a vast array of previously intractable non-model organisms (1), but nearly all prior work has focused on how mutations spread among well-individuated organisms (*i.e.*, a life cycle that includes regular genetic bottlenecks), ignoring the effects of within-organism somatic mutations. This is a reasonable assumption for animals, in which germ cells segregate early during ontogeny, but many multicellular organisms (*i.e.*, plants, fungi, red algae, brown algae) do not have germline sequestration (2, 3).

Clonal reproduction offers many ecological advantages. In addition to persisting over long timescales, horizontal growth through root or mycelium expansion also facilitates large spatial colonization. This effective use of clonal growth in diverse environments is exemplified by seagrasses, with genets spanning large areas of shallow waters despite local fragmentation (4). Similarly, a 2500-year-old clone of the fungus *Armillaria gallica* spread over 75 hectares of forest floors, sustained by its ability to feed on dead wood (5). Clonal proliferation through structures like stolons or rhizomes enhances colonization, especially after disturbances, such that many of these organisms have pioneering roles in their ecosystems. For instance in *P. tremuloides*, the growth of

Significance Statement

This study enhances our understanding of evolutionary processes in long-lived clonal organisms by investigating somatic mutation accumulation and dispersal patterns within the iconic Pando aspen clone. The authors estimated the clone to be between 10,000 and 80,000 years old and uncovered a modest spatial genetic structure in the 42.6-hectare clone, suggesting localized mutation build-up rather than dispersal along tissue lineages. This work sheds light on an ancient organism and how plants may evolve to preserve genetic integrity in meristems fueling indefinite growth, with implications for our comprehension of adaptive strategies in long-lived perennials.

Author affiliations: ^aSchool of Biological Sciences, Georgia Institute of Technology, Atlanta, USA; ^bUniversity of Chicago, Chicago, USA; ^cDepartment of Wildland Resources, Utah State University, Logan, USA; ^dEcology Center, Utah State University, Logan, USA; ^eSchool of Environment, Society and Sustainability, University of Utah, Salt Lake City, USA; ^fEarth and Environmental Sciences Division, Los Alamos National Laboratory, Los Alamos, USA; ^gDepartment of Biology, Utah State University, Logan, USA

RMP, KM, ZG and WCR conceived the study. RMP, AP and KM sampled the Pando clone data. JM, VK and AV sampled and analyzed the pollen data. RMP and ZG performed the analyses. RMP, ZG and WCR wrote the paper. All authors read and approved the manuscript before submission.

Authors declare no competing interests.

¹To whom correspondence should be addressed. E-mail: rozennpineau@uchicago.edu, zach.gompert@usu.edu

125 new ramets is stimulated by nutrients and light availability in
126 areas recently damaged by fire (6, 7). Clonal propagation, as
127 opposed to sexual reproduction, might also offer evolutionary
128 advantages in challenging environments marked by pollinator
129 scarcity or conditions inhibiting seed germination. The survival
130 of the largest known clone of slow-growing rhizomatous sedge
131 *Carex curvula* in alpine terrain may indeed have endured
132 thanks to clonal recruitment (8). The persistence and
133 ecological dominance of these clonal organisms underscore the
134 evolutionary benefits of modular growth in ensuring survival
135 and success across diverse habitats.

136 Yet, because every cell division represents an opportunity
137 for DNA replication errors, clonal organisms also have greater
138 opportunities to accumulate mutations. Indeed, the number
139 of cell divisions separating the basal from the apical meristems
140 may lead to the buildup of somatic mutations, spreading to
141 derived tissues (9). While the emergence of somatic mutations
142 in animals can lead to lethal cellular proliferation (tumors),
143 it is noteworthy that the longest documented lifespans are
144 all clonal organisms. In seagrasses, such as *Posidonea*
145 *australis* (10), *P. oceanica* (11), *Thalassia testudinum* (4),
146 or *Zostera marina L.* (12), estimates suggest ages exceeding
147 6000 years. With indefinite growth, the longevity of the clone
148 is independent from the module life span, making it potentially
149 immortal. Furthermore, clonal reproduction implies that
150 somatic mutations can be passed down to their progeny,
151 making somatic mutation an important mechanism of creating
152 heritable variation for Darwinian evolution by natural selection.
153 Indefinite growth, long lifespans and clonal reproduction are
154 thus combined opportunities for mutation accumulation in
155 clonally long-lived organisms.

156 The genetic signal from somatic mutations in clonal
157 organisms can be harnessed to track within-plant architecture,
158 but also the evolutionary history of the organism (13). So
159 far, the study of the accumulation and spread of somatic
160 mutations has been limited to a few studies in plants and
161 fungi (4, 6, 14, 15), such that we still know little about the
162 evolutionary fates of intra-organism mutations in large and
163 long-lived perennials.

164 Here, we focus on one of the largest clonally-reproducing
165 organism, the Pando clone, a quaking aspen that is also
166 believed to be one of the oldest still-living organism. Quaking
167 aspen (*Populus tremuloides*) can reproduce vegetatively by ex-
168 panding roots from which new ramets grow. While individual
169 stem lifespan averages 110 years (16), clones can regenerate
170 themselves from the root stock such that the organism can
171 be far older than its parts. The Pando clone has gathered
172 particular attention for its size (42.6 hectares comprising
173 ~47,000 individual stems) and was even nicknamed “Pando”
174 (Latin for “I spread”) for this reason (17, 18).

175 To explore the evolutionary history of the Pando clone,
176 we sequenced leaves, roots and bark samples at both large
177 and fine scales. After identifying the samples pertaining to
178 Pando, as opposed to the neighboring clones, we isolated
179 the somatic mutations within the clone. Only the somatic
180 mutations were considered, as germline mutations are present
181 in every ramet and will not inform spatial expansion and
182 genetic patterning. To increase confidence in the SNP-calling
183 of somatic mutations and account for missing mutations, we
184 used a technical replicate sequencing approach. Comparing
185 both large scale and finer scale datasets, we find that physically

187 close ramets tend to be genetically more similar. Using
188 phylogenetic models, we estimate the age of the Pando clone to
189 range from ~16,000 to 80,000 years, making it one of the oldest
190 living organisms on Earth. In addition to shedding light on an
191 old and iconic organism, this work deepens our understanding
192 of the rate of accumulation and spread of somatic mutations
193 within long-lived perennials.

194 Results

195 **Brief overview of the different datasets.** To describe the evolution-
196 ary history of the Pando clone, we generated three different
197 sets of data using different spatial scales and sequencing
198 strategies (Table 1). We generated a large scale dataset by
199 sampling leaves from the whole Pando stand, comprising the
200 neighboring non-Pando clones, on a 50-m grid (“large scale
201 dataset”, 184 samples, 22,888 SNPs, Supplementary Figure
202 A.2, left panel). To focus on a smaller spatial scale and
203 different tissue types, we gathered samples from two additional
204 subsections from within the Pando clone and sequenced root,
205 bark, leaves and branches (“fine scale dataset”, 101 samples,
206 15,925 SNPs with 3034 somatic mutations, Supplementary
207 Figure A.2, right panel). To avoid batch effects and possible
208 confounding effects of the two different spatial scales, the
209 large and fine scale datasets were analyzed separately (see
210 ordination plots in Supplementary Figure A.1).

211 Finally, to test our ability to accurately identify somatic
212 mutations, we re-sequenced 12 samples from the fine scale
213 dataset 8 times (same DNA extraction sequenced 8 times)
214 (“replicate dataset”, 80 samples with 101 somatic mutations).

215 **Delineating the Pando clone.** To isolate the Pando clone
216 samples from the neighboring clone samples in the large
217 scale dataset, we applied an ordination method and k-means
218 clustering on 22,888 single nucleotide variants comprising a
219 mixture of germline SNPs and somatic mutations (principal
220 component analysis, PCA, Figure 1A). Pando samples (89
221 out of 184 samples) formed a distinct cluster in PCA space
222 with spatial boundaries for Pando that were consistent with
223 previously defined clone boundaries based on morphological
224 differences (19), and microsatellite markers (17, 20) (Figure
225 1B). We thus verified the spatial extent, 42.6 ha, of Pando.

226 **Identifying the somatic mutations.** Germline mutations are
227 inherited and should be common to Pando as a whole. Somatic
228 mutations, however, are mutations that appeared after seed
229 formation and during the organism’s growth, potentially
230 making tractable the evolutionary history of the organism. To
231 describe the development of the Pando clone in time and space,
232 we thus focused on the somatic mutations in a large number
233 of samples. With a genome size of 480 Mbp (21), sequencing
234 whole genomes for hundreds of individuals was prohibitively
235 expensive. Furthermore, we only needed information from the
236 same subset of the genome for a high number of individuals.
237 Hence, we generated a reduced complexity library using
238 Genotyping-By-Sequencing (GBS) (22).

239 Somatic mutations have been extensively studied in the
240 context of cancer research (23), which are caused by post-
241 zygotic mutations. In such cases, one common approach to
242 identify somatic mutations in tumor cells is to compare the
243 genomes of a set of healthy cells (“normal”) and a set of
244 malignant cells (“tumor”). However, in our case, we did not
245

249
250
251
252
253
254

311
312
313
314
315
316
317
318
319
320

255 **Table 1.** To study the evolutionary history of the Pando clone, we generated datasets at different spatial scales and using different sequencing
256 strategies. The large scale and fine scale datasets have the same initial number of mutations as the variant calling was done on both sets at
257 once.

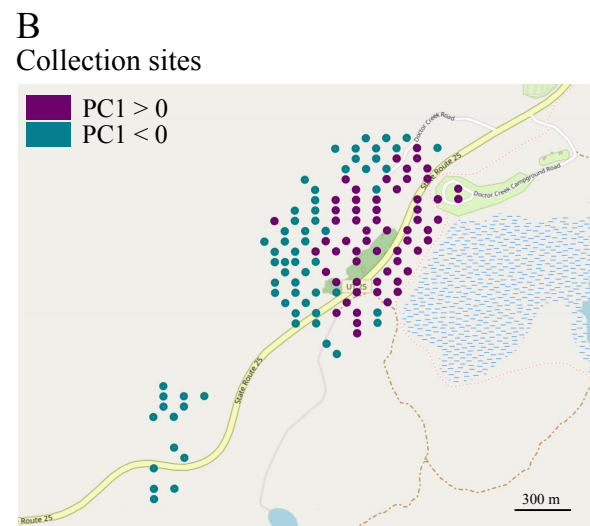
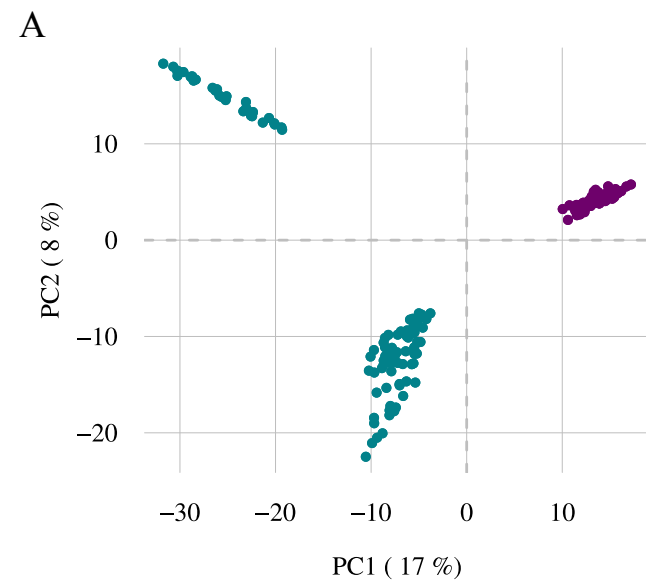
258
259
260
261
262
263
264

321
322
323
324
325
326
327
328
329
330
331
332
333
334
335
336
337
338
339
340
341

Dataset name	Number of samples	Number of mutations (all/somatic)
large scale	184 (Pando and neighboring clones)	22,888/-
	89 (Pando only)	15,925/3942
fine scale	101	15,925/3034
replicate	80	4,607/101

265
266
267
268
269
270
271
272
273
274
275
276
277
278
279

327
328
329
330
331
332
333
334
335
336
337
338
339
340
341



301 **Fig. 1.** Parsing out the Pando samples from the surrounding clone samples. (A) The projection of genotypes (22,888 variants) form three distinct clusters: two clusters with
302 negative PC1 values and one cluster with positive PC1 values. Points are labeled with a color proportional to their PC1 value. (B) Plotting the PC1 value into the sampling
303 space delineates the Pando cluster (positive PC1 values) from the surrounding clone clusters (negative PC1 values).

304
305
306
307
308
309
310

363
364
365
366
367
368
369
370
371
372

373 have access to the “normal” set of samples, which would be
374 the initial “mother” tree of the Pando clone. Thus, to separate
375 somatic mutations from the pool of genetic variants, we created
376 a set of “normal” samples based on the variants found in the
377 neighboring clones and in 100 *P. tremuloides* samples from
378 the USA’s Intermountain region (Colorado, Wyoming, Nevada,
379 Idaho). We removed variants that were found in both the
380 Pando clone samples and this comparative dataset, with the
381 reasoning that common mutations may be germline in origin,
382 or highly mutable sites. Secondly, to minimize the effects of
383 sequencing errors, we removed mutations that were found in
384 only one sample.

385 With an inherent per-base pair error rate of approximately
386 0.31% for Illumina reads (24), focusing on rare (somatic)
387 mutations increases the risks of missing true mutations, and on
388 picking false mutations. To assess our ability to consistently
389 recover somatic mutations, we sequenced the same sample
390 several times (12 samples sequenced 8 times each, from the
391 same DNA extraction). After applying basic quality filtering
392 (see Methods for more details), we kept the mutation as somatic
393 if it was found in at least two replicates of a sample, and at
394 most 80% of the samples (Figure 2A). This decision for the
395 80% filter was based on the rationale that variants occurring
396 in more than 80% of the ramets are likely germline mutations,
397 shared across all trees but not necessarily detected in each one.
398 These filters left us with a set of 101 mutations present in less
399 than 40% of the samples, as there were no mutations between
400 40% and the 80% cutoff (Figure 2B). When a mutation is
401 found in two replicates per sample, it is on average found
402 in 3.5 replicates total (i.e., 44% of the replicates), which is
403 significantly higher than by chance (randomization test, null
404 expectation = 0.37 with 1000 permutations, $P < 0.001$, Figure
405 2C). The replication of mutations did not vary as a function
406 of coverage (Supplementary Figure A.4). While these analyses
407 confirm the detection of somatic mutations, they suggest that
408 some mutations are still being missed. We revisit this issue
409 when estimating the age of Pando (see Age of the Pando clone
410 section).

411 Having established our ability to recover rare mutations,
412 we proceeded to identify somatic mutations in the rest of the
413 Pando datasets, which include both the large-scale dataset
414 (with only the Pando samples) and the fine-scale dataset (Table
415 1). We applied the same set of filters that were applied to the
416 replicate dataset to filter out the germline mutations.

417 **Patterns of spatial genetic structure for somatic mutations -**
418 **large scale.** We identified 3942 putative somatic mutations
419 from the 89 Pando ramet samples (large scale dataset, Table
420 1). On average, samples shared 26.8% somatic mutations
421 (range = 583 to 1679). Due to clonal reproduction and spatial
422 restriction in dispersal (roots from one tree can expand up
423 to 15m (25)), we expected to observe a non-random spatial
424 distribution of somatic mutations (26). More specifically,
425 we expected ramets that are close in space to share more
426 mutations than ramets that are further apart from each
427 other. However, there was only a marginally detectable
428 correlation between the proportion of shared variants and the
429 physical distance between pairs of ramets (Figure 3A,
430 Pearson correlation coefficient = -0.02, $[CI] = [-0.05, 0.00]$,
431 Figure 3B, null expectation = -0.001 with 1000 permutations
432 of the somatic mutation set, $P < 0.001$). We uncovered further
433 spatial structure when focusing on spatial distribution of each

434 somatic mutation. The mean distance between all samples
435 sharing a mutation, averaged over all mutations, is smaller
436 than expected by chance (Figure 3C&D, mean distance for
437 groups sharing a somatic mutations is 264.28 m, as compared
438 to the mean distance (null expectation) of 279.93 m for a
439 randomized dataset with 500 permutations of the sample
440 coordinates, $P < 0.002$). Given that a single root can extend
441 up to 15 m in space (25), and our grid sampling had a minimum
442 distance of 50 m, we hypothesized that we might be missing
443 spatial signals at finer scales. Additionally, focusing solely on
444 leaves could overlook somatic mutation signals, as clonal aspen
445 expand through their roots (Figure 4). To better understand
446 the spread of somatic mutations within and between ramets
447 and tissue types, we conducted our analyses at a finer spatial
448 scale by comparing samples from sub-sections of the clone and
449 from different tissues within ramets.

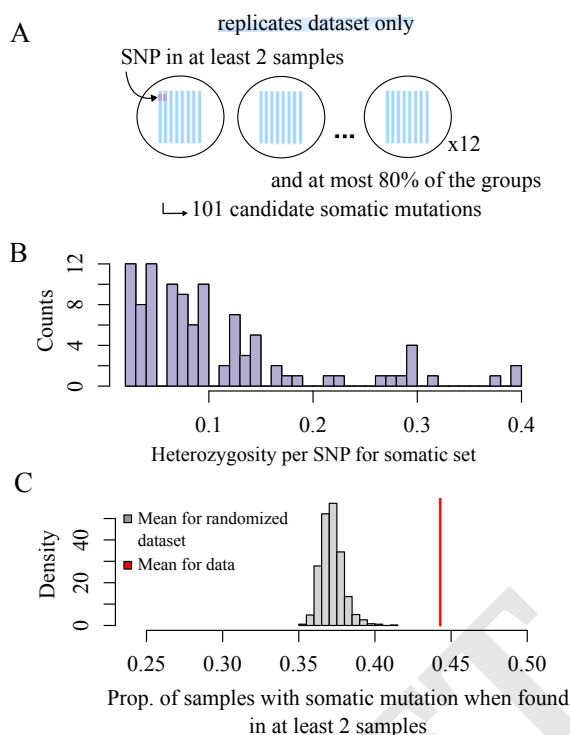
450 **Patterns of spatial genetic structure for somatic mutations -**
451 **fine scale.** To detect fine-scale spatial structure and differences
452 between tissue types, we focused on a smaller spatial scale,
453 sampling ramets 1-15 m apart in a circular scheme at
454 two locations within the Pando clone (~120 m apart, see
455 Supplementary Figures A.2 and A.3), as well as tissues within
456 ramets (roots, shoots, branches, and leaves).

457 Overall, we found significant evidence of genetic structure,
458 with genetic differences increasing with spatial distance (Figure
459 5A, Pearson correlation coefficient = -0.1, $[CI] = [-0.12, -0.07]$,
460 null expectation = 0.00 with 500 permutations, $P = 0.006$).
461 The signal was especially strong for leaves (Pearson correlation
462 coefficient -0.44, $[CI] = [-0.49, -0.38]$), with more somatic
463 mutations shared between spatially close leaves compared to
464 random ($P < 0.001$). The roots also shared significantly
465 more mutations than expected under a null distribution
466 (Pearson correlation coefficient -0.11, $[CI] = [0.18, -0.03]$,
467 $P = 0.026$ when compared to null distribution). This signal
468 was not observed in the branches and the shoots (Pearson
469 correlation coefficient -0.06, $[CI] = [-0.24, 0.11]$ for branches
470 and -0.05, $[CI] = [-0.37, 0.28]$ for shoots).

471 Similarly, a variant-level approach showed that the number
472 of shared somatic mutations per pair of samples decreased
473 with spatial distance (Figure 5B, mean distance for groups
474 sharing a somatic mutations is 46.33 m, as compared to the
475 mean distance (null expectation) of 55.31 m for a randomized
476 dataset with 500 permutations, $P = 0.002$). The leaves showed
477 the strongest spatial structure signal using this metric (Figure
478 5B and Supplementary Figure A.5), while other tissue types
479 did not differ from the null expectation. The absence of signal
480 in the shoots and branches may be partly explained by the
481 significantly higher number of mutations recovered in leaves
482 compared to other tissues (Supplementary Figure A.8).

483 **Age of the Pando clone.** We took a phylogenetic approach to
484 infer the Pando clone age with our set of somatic mutations.
485 Specifically, we reconstructed the phylogenetic history of the
486 Pando samples with BEAST2 with the large-scale dataset
487 (3957 mutations and 102 samples). We used a variable
488 population size coalescent model, which reconstructs the past
489 population dynamics based on a contemporary set of sequence
490 data (Coalescent Bayesian Skyline model in BEAST2 (27)).
491 Because the somatic mutations are rare, they can be harder
492 to detect using Illumina technology when the read depth is
493 not exceptionally high (mean read depth is 14 \times). To estimate
494

497
498
499
500
501
502
503
504
505
506
507
508
509
510



524 **Fig. 2.** Replication power for somatic mutations. (A) To filter for somatic mutations, we kept the mutations that were found in at least two samples per replicate group, and at 525 most 80% of the samples (see methods for details on the filters). We identified 101 somatic mutations, (B) found in less than 40% of the individuals. (C) If a mutation is present 526 in two samples in a group, it is found on average in 44% of the samples total.

527
528
529 the proportion of missed mutations, we compared the set 530 of somatic mutations obtained in the replicate dataset (101 531 mutations, Figure 2), to the set of somatic mutations obtained 532 in the same samples in the main dataset, where each of samples 533 was sequenced only once (3957 mutations). Only $\sim 6\%$, 6 534 mutations out of 101 were replicated. Coverage partially 535 explained this lack of replication: in general, mutations that 536 were found in the replicate dataset had higher depth than 537 mutations found in the fine scale dataset (41.5x 538 versus 11.6x), however, some of the somatic mutations that 539 were found in both datasets had a depth as low as 6x for the 540 fine scale dataset (Supplementary Figure A.7). It is important 541 to note that the mutations were called independently in these 542 two datasets. Given that variant calling is influenced by sample 543 composition, this independent variant call may underestimate 544 the mutation replication rate.

545
546 To take into account the effect of large amount of missing 547 mutations on the phylogenetic tree height and thus the Pando 548 clone age, we empirically estimated the relationship between 549 the proportion of missing mutations and the phylogenetic tree 550 height (Figure 6A). To do so, we randomly removed mutations 551 and simulated the phylogeny in BEAST (black dots, Figure 552 6A). We obtained a linear relationship between the proportion 553 of missing mutations and the phylogenetic tree height, which 554 we extrapolated to take into account false negatives or positives 555 (i.e. mutations that we either missed, or called but are not 556 real). This scaled tree height was converted to years based 557 on the published estimation of somatic mutation rate in *P.* 558 *tremuloides* (28) using the following equation:

$$age(\text{years}) = \frac{Tn_S}{n_{BP}} * \frac{3}{\mu}$$

559 with T being the scaled phylogenetic tree height, n_S the total 560 number of mutations, n_{BP} , the total number of base pairs 561 sequenced, μ the leaf somatic mutation rate ($1.33 * 10^{-10}$ per 562 base per haploid genome per year (28)), taking into account 563 that the Pando clone is triploid (20, 29) (see Methods for 564 details).

565 We calculated three different estimates of the Pando clone 566 age based on three different assumptions (Figure 6B). First, 567 if the mutations we detected are all true positives and we 568 did not miss any somatic mutations in the proportion of the 569 genome we sequenced, we do not have to apply any correction 570 to the phylogeny height conversion and the Pando clone would 571 be about 34,000 years old (assumption 1, $sd = 1007$ years). 572 Second, if we take into account that we only detected 6% of the 573 somatic mutations present in the samples and use the linear 574 relationship (Figure 6A) to account for false negatives, then 575 the clone would on average be 81,000 years old (assumption 576 2, $sd = 1922$ years). Finally, if only 6% of the mutations we 577 detect are true positives, the Pando clone would be 16,402 578 years old (assumption 3, $sd = 7$ years). The population 579 dynamics reconstruction suggest a slow and steady increase 580 during the first half of Pando's life, followed by a steadier 581 population size (Figure 6C). The unit of effective population 582 size here can be thought of in terms of cellular lineages giving 583 rise to new tissues (as compared to individuals when working 584 with germline mutations). Despite its thousands of years of 585 history, the phylogeny of the Pando clone samples suggests only 586

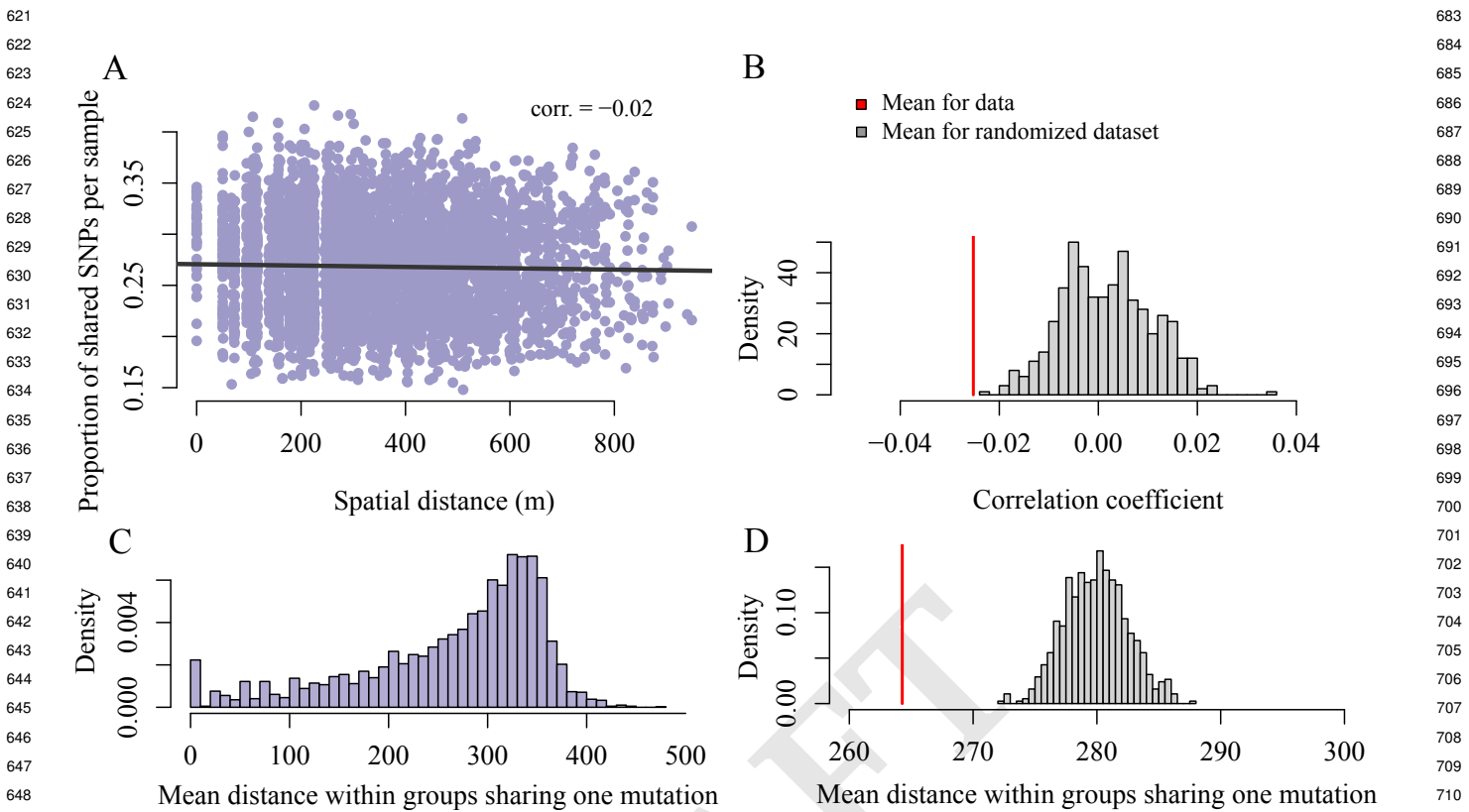


Fig. 3. Detecting spatial genetic structure at large scale. (A) We use the set of 3942 somatic mutations identified in the Pando clone samples to test for spatial genetic structure. Focusing on the sample-level, we observe that the number of shared variants between pairs of samples decreases with the physical distance between samples pairs (Pearson correlation coefficient between number of variants and spatial distance is -0.02 , $[CI] = [-0.05, 0.00]$), which is significantly different from a randomized distribution ($P < 0.001$) (B). (C & D) Focusing on the variant-level, we find that the mean distance within a group of samples sharing the variant is significantly less than expected by chance (mean distance for data is 264.28 m and mean distance for randomized dataset is 279.93 m, $P < 0.001$).

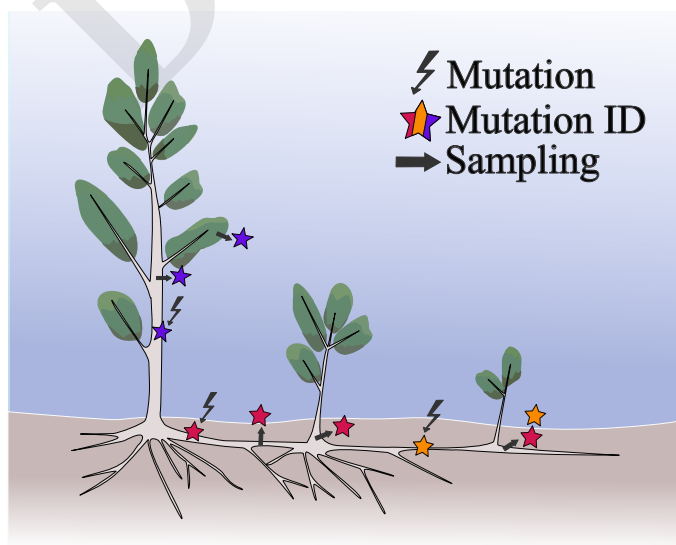


Fig. 4. Conceptual model of somatic mutation inheritance between ramets within an aspen clone. When a mutation arises, we expect it to propagate down to the new tissues as the clone continues to grow. New mutations are symbolized with the lightning bolt. The mutation identity is marked as a colored star and the dark marks corresponds to where samples could be collected from the clone.

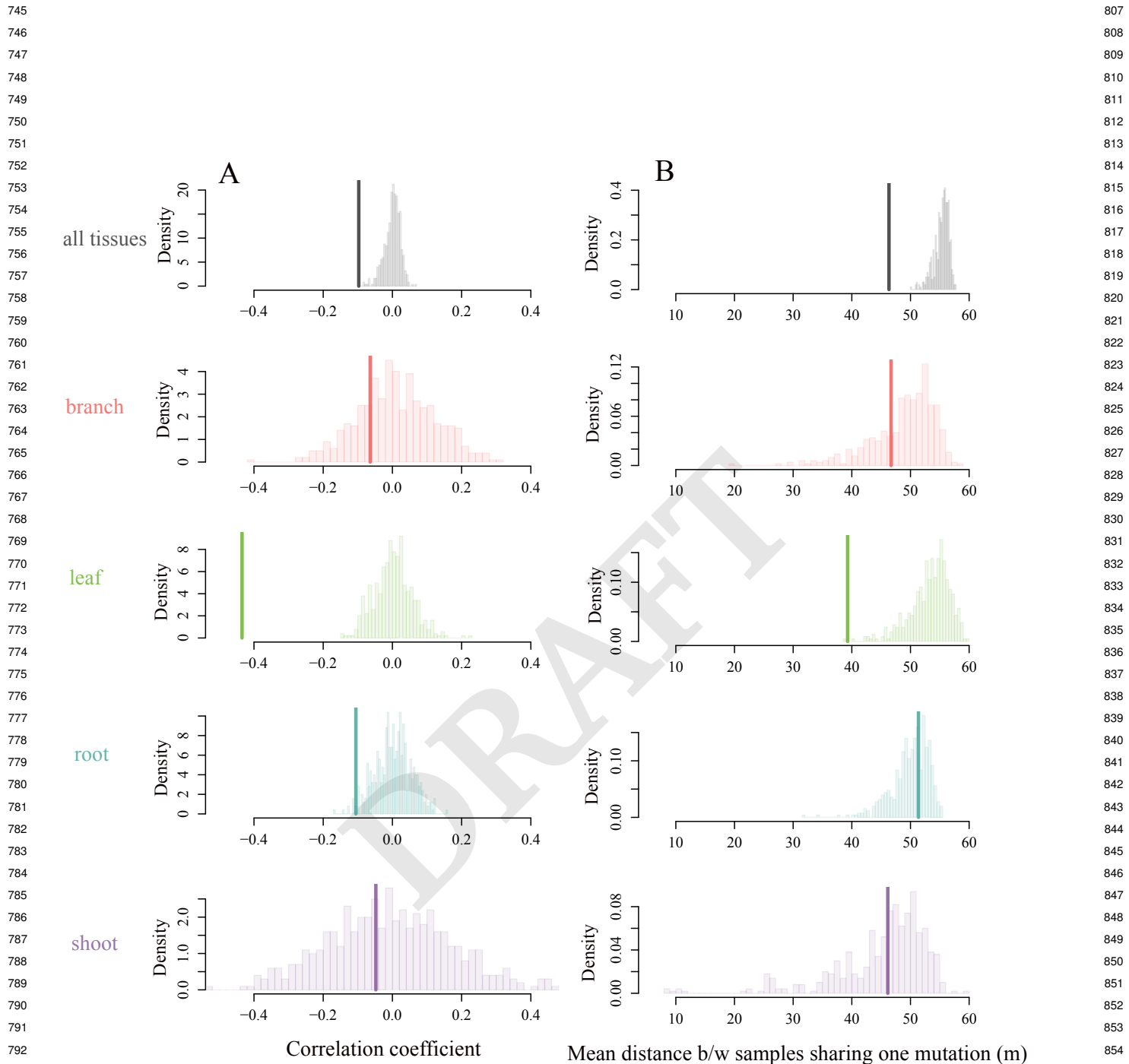


Fig. 5. Detecting spatial genetic structure at the finer scale. We use the set of 3034 somatic mutations detected in the finer scale dataset to test for smaller-scale and within tissues spatial genetic structure. (A) Focusing at the sample-level, we observe an overall significantly negative correlation between genetic and physical distance (thick lines, Pearson correlation coefficient = -0.097 , $[CI] = [-0.12, 0.07]$), driven mostly by the leaves and the roots (compared to null distributions, $P < 0.001$ and $P = 0.026$, respectively). (B) Focusing on the variant-level, we find that the mean distance within a group of samples sharing the variant (thick line, mean distance for the data is 46.33 m) is significantly less than expected by chance when considering all tissue types together (mean distance for the null distribution is 55.31 m, $P < 0.001$), signal that is mostly driven by the leaves (mean distance for leaves only is 39.28 m, as compared to 53.36 m expected under the null distribution, see Supplementary Figure A.6 for means and p-values).

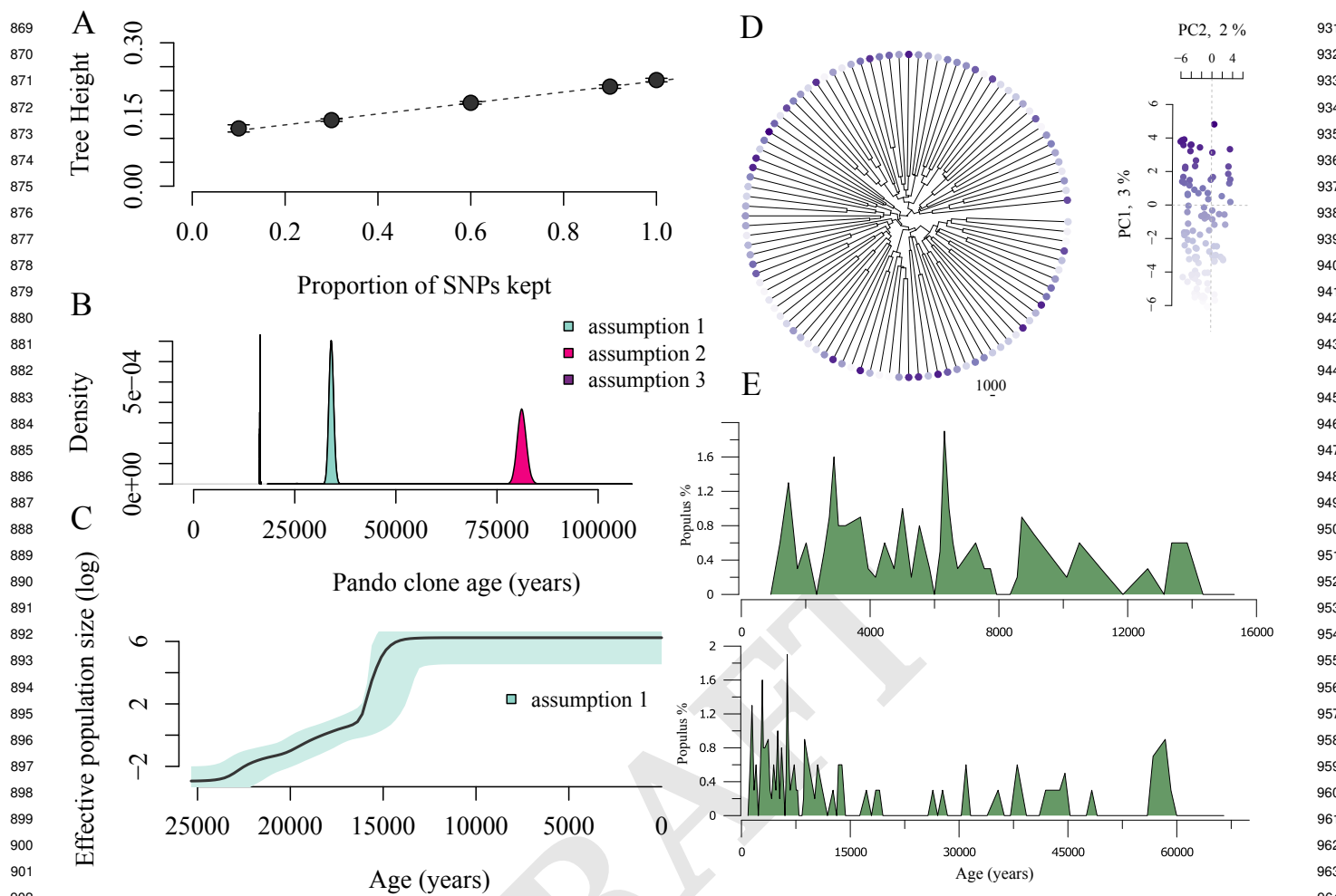


Fig. 6. The Pando clone is at least 16,000 years old. (A) We use the relationship between the proportion of missing mutations from a simulated dataset and the phylogenetic tree height to take into account the somatic mutations that we might be missing in the Pando clone (linear regression $y = 0.10 + 0.11x$, $P < 2.2e - 16$, $R^2 = 0.92$). (B) With this correction, we calculate the Pando clone age based on three different assumptions: (1) if the mutations we detect are all real, the Pando clone would be about 34 000 years old ($\pm sd = 1007$ years); (2) if we are missing 94% of the mutations, then the clone would on average be 81,000 years old ($\pm sd = 1922$ years); (3) finally, if only 6% of the mutations we detect are real somatic mutations, the Pando clone would be 16,402 years old ($\pm sd = 7$ years). (C) The Bayesian skyline plot suggests a steady population increase followed by a plateau. Note that this example was scaled for assumption 1 (all the mutations that we detect are real somatic mutations). (D) Despite thousands of years of evolutionary history, the Pando clone shows minimal phylogenetic structure (points colored according to PC1 score). (E) Pollen records from the Fish Lake show *Populus* was consistently present during the last 15,000 years, and generally well-represented over the last 60,000 years.

minimal structure (Figure 6D). The same analysis of the fine scale dataset suggests results of a similar scale, that is, an age for Pando between $\sim 10,000$ and $100,000$ years (Supplementary Figure A.9). Interestingly, pollen records from the Fish Lake support a continuous presence of *Populus* during the last 15,000 years, potentially up to 60,000 years ago, which generally coincides with our age estimates for Pando (Figure 6E).

Discussion

We explored the evolutionary and developmental history of a long-lived, clonally reproducing tree, confirming that the Pando clone consists of a single genet spanning 42.6 hectares. We based our estimate of the age of the Pando clone on the accumulation of somatic mutations, acknowledging uncertainties due to rare mutation calls by exploring three different scenarios (Figure 6). Our most conservative estimate, based on the percentage of mutations we are confident in recovering, suggests the clone is at least 16,000 years old. A

second scenario, using all detected mutations without further filtering, places the clone's age at approximately 34,000 years. Lastly, our least conservative estimate, which includes potential undetected somatic mutations, suggests the Pando clone could be as old as 81,000 years. Regardless of the scenario, these estimates highlight the remarkable longevity of the Pando clone, which has likely persisted for more than ten thousand years, making it one of the oldest living organisms on Earth.

The last glaciation event models that this region of North America at low altitudes was not covered in ice (30, 31). With an altitude of 2700 m however, the specific area where the Pando clone is in the Fish Lake plateau could have been caught in mountain glaciers. Boulder exposure ages in the Fish Lake plateau suggests a local last glacial maximum of 21,100 years (32). However, the Fish Lake Plateau glaciers reconstructed from models have altitudes ranging from 2950 to 3190 m, thus higher in elevation than the Pando area, suggesting that vegetation survived through the glacial period, specifically at

993 Pando's present location. This interpretation is supported by
994 subfossil pollen analyzed from a lake sediment core collected
995 nearby Fish Lake (Figure 6E, upper panel). This data show
996 that *Populus* pollen has been present continuously in the Fish
997 Lake catchment for the last 15,000 years but has been generally
998 present over the last 60,000 years.

1000 When reflecting on the Pando clone's expansive territorial
1001 dominance and enduring resilience, its triploid nature may
1002 have played a crucial role in its success (33). Polyploid
1003 organisms, like Pando, often exhibit advantages such as en-
1004 hanced adaptability and competitive ability, traits commonly
1005 associated with the success of invasive species. Although
1006 polyploidy can be energetically costly, it is frequently linked to
1007 rapid territorial expansion (34). Prior work shown a positive
1008 correlation between polyploidy and plant invasiveness, along
1009 with a reduced risk of endangerment (35). In Pando's case,
1010 polyploidy may have contributed to its capacity to thrive in
1011 changing environments and secure its long-lived dominance.
1012 However, unlike many polyploid species that spread via sexual
1013 reproduction, odd-numbered ploidies have typically very low
1014 fertility, making clonal evolution even more critical to Pando's
1015 persistence (36). This highlights the importance of somatic
1016 mutation and within-organism evolution in shaping the genetic
1017 diversity and resilience of this ancient clone.

1018 To explore isolation by distance in clonally reproducing
1019 organisms, we sequenced leaves across a 50-m grid covering
1020 the entire Pando area as well as leaves, branches, shoots and
1021 roots at a finer scale, with samples collected 1-15 m apart in
1022 two locations within the clone. Our findings reveal spatial
1023 genetic structure within the clone, with samples sharing more
1024 mutations when geographically closer (Figure 3 & 5). While we
1025 were able to detect this spatial signal at fine scale in the leaves
1026 and roots, it was weaker at larger scales than expected and
1027 usually observed in clonal organisms (26, 37, 38). Although we
1028 can clearly distinguish Pando samples from neighboring clones
1029 (Figure 1) and detect some internal structure within Pando
1030 (Figures 3&5, the relatively low number of shared mutations
1031 between closely related tissues (roots, shoots and branches,
1032 Figure 5) suggests an intriguing underlying dynamic.

1033 Research on within-clone mutation diversity shows that
1034 members of the same clonal population are rarely genetically
1035 identical, but rapidly accumulate mutations that are not
1036 shared by all individuals (12). Similar observations were
1037 made in strawberries where mutations present in mother
1038 plants were absent in daughter plants propagated via stolons
1039 (13). Somatic mutations occurring in local tissues are not
1040 always passed down to the next generation of cells. As
1041 roots grow, the meristematic island that will give rise to
1042 new ramets gets pushed by waves of cells, protecting the
1043 stem cells from mutation accumulation (39). This aligns with
1044 the low number of somatic SNPs detected between two oak
1045 leaf genomes sampled from the same individual (17 out of
1046 314 865 putative SNPs in 236-yr oak tree (15)). Despite
1047 prolonged lifespan and exposure to significant environmental
1048 changes, plants seem to have evolved mechanisms protecting
1049 the meristems from accumulating mutations. When sequencing
1050 entire tissues, we might be observing the localized buildup of
1051 somatic mutations rather than the cell lineages contributing
1052 to organismal evolution, which would explain the relatively
1053 weak spatial genetic structure.

1055 Our results suggest differing rates of somatic mutations be-
1056 tween tissues that contribute to the progeny versus those that
1057 do not, and between annual and perennial tissues. We found
1058 that leaves accumulate more mutations than bark (branches
1059 and shoots), and roots. This aligns with findings from other
1060 studies, where longer-lived organs show lower mutation rates
1061 compared to more short-lived structures (leaves versus petals)
1062 (13). Similarly, in peach trees, mutation accumulation in
1063 branches—tissues involved in sexual reproduction—was lower
1064 than in roots (13), suggesting a history of selection minimizing
1065 mutation accumulation in reproductive tissues.

1066 This work provides novel insights into the evolutionary
1067 history of one of Earth's oldest and largest known organisms,
1068 the quaking aspen clone Pando. By analyzing somatic
1069 mutations across different spatial scales and tissue types, we
1070 estimate the clone's age to be at least 16,000 years old, with
1071 potential upper estimates reaching 80,000 years. Our findings
1072 reveal a weaker than expected spatial genetic structure within
1073 the clone, suggesting localized mutation build-up rather than
1074 consistent dispersal along tissue lineages. This work advances
1075 our comprehension of intra-organism evolution in clonal plants
1076 and suggests potential mechanisms for maintaining genetic
1077 integrity in indefinitely growing organisms. The observed
1078 differences in mutation accumulation between tissue types
1079 provide insight into how plants may evolve to preserve the
1080 genetic fidelity of meristems fueling indefinite growth. These
1081 findings have broader implications for our understanding of
1082 adaptive strategies in long-lived perennials and the evolution-
1083 ary dynamics of clonal organisms in changing environments.

1084 Methods

1085 **Sampling.** The Pando clone (*Populus tremuloides*) is located
1086 in the Fishlake National Forest, Utah, USA (38°31'N,
1087 111°45'W), and ranges in altitude from 2700–2790 m. The
1088 sampling area consists of two distinct subsections dominated
1089 by aspen containing both Pando and surrounding clones.
1090 The large scale dataset containing the Pando clone and the
1091 surrounding clones was obtained by collecting leaves based
1092 on a 50-m grid in June 2006 and November 2007, sampling
1093 from both a smaller (younger) and a taller (older) tree at
1094 each location (see (17) for more details). To test for the finer
1095 scale within clone genetic structure, leaves, roots, bark from
1096 the trunk and branches of additional stems were sampled in
1097 June 2022. Two sampling sites within the Pando clone were
1098 chosen for this additional sampling, one situated in an area
1099 that was clear-cut 30 years ago and the other one in an older
1100 area (Supplementary Figures A.2 and A.3). 100 additional
1101 leaf samples were collected from *P.tremuloides* in the USA's
1102 Intermountain region (Colorado, Wyoming, Nevada, Idaho)
1103 to generate the 'panel of normals' (see "Identifying somatic
1104 mutations" section). Leaves were kept in paper coin envelope
1105 and placed in desiccant. Root and bark samples were placed
1106 in polyethylene bags and kept at cool temperatures before
1107 long term storage at -20°C.

1108 **Sequencing.** The 296 leaf samples from the Pando and
1109 surrounding clones, and the 45 root samples, 45 leaves and
1110 27 bark samples from trunk and branches were prepared
1111 for GBS sequencing. Woody tissues were powdered using a
1112 pestle and mortar and further lysed using Tissue Lyzer II
1113

(TissueLyser II, Qiagen). Genomic DNA was extracted using the DNeasy Plant Pro Kit (Cat. No. 69204, Qiagen). To generate a reduced complexity DNA library, the genome was digested using *Mse*I and *Eco*R1 enzymes. The fragments were labelled and prepared for sequencing using oligonucleotides consisting of Illumina adaptors and unique 8-10 base pair (bp) sequences. The fragments were amplified and size-selected to only keep fragments between 300 and 400 bp-long, before sequencing (Genotyping-By-Sequencing, see (40) for more details). The samples were sequenced at the University of Texas Genomic Sequencing and Analysis Facility (Austin, TX, USA). Library preparation and sequencing were done in three batches, with 367 samples sequenced with an Illumina HiSeq 4000 (1×100 base pair reads) in 2018, 126 and 96 samples sequenced on a NovaSeq (1×100 base pair reads) in 2022 and 2024, respectively (one lane each). Total number of reads was 1 027 955 624.

Genome alignment and variant calling. We used the mem algorithm from bwa (default options, version 0.7.17-r1188, (41)) to align the reads to the published reference genome for *P. tremuloides* (21). We used samtools to compress, sort and index the alignments (Version: 1.16 (41)). We called the variants using samtools mpileup algorithm (Version: 1.16). The large-scale and fine-scale datasets were pooled for variant calling, and the replicate and 'panel of normals' datasets were kept separate. We kept mapped reads with a quality >30 , skipped bases with base quality >30 and ignored insertion-deletion polymorphisms. At this step, we also separated from the pooled vcf the fine-scale and large-scale samples. We then filtered our set of SNPs by keeping the sites for which we had data (mapped reads) in at least 60% of individuals, a mean coverage per sample of at least $4\times$, and at least one read supporting the non-reference allele. We also removed SNPs failing the base quality rank-sum test ($P < 0.005$), mapping-quality rank-sum test ($P < 0.005$), and the read position rank-sum test ($P < 0.01$).

To minimize confounding batch effects, we additionally removed the variants that had a notable difference in coverage between the fine-scale and large-scale datasets. Indeed, differences during the GBS size selection step between batches could lead to differences in the representation of some fragments. To counter this, we removed SNPs with a difference in coverage between the two datasets, that was more than half the mean coverage of the datasets combined (the mean coverage was $14\times$ per individual per variant). At this step, we were left with 22,888 variants.

In order to differentiate between the samples pertaining to the Pando clone and the surrounding clones, we obtained Bayesian estimates of genotypes. We specifically computed the posterior mean genotype as a point estimate based on the genotype likelihood from bcftools and a binomial prior based on the allele frequency estimates from the vcf file. We used principal component analysis (PCA) to ordinate the samples; this was performed on the matrix of centered but not scaled genotype estimates. We did not scale as the variance was similar between samples. The PCA clustered the samples, separating the Pando clone samples, from the surrounding clone samples (Figure 1). We used k-means clustering (R kmeans function, with K=2) to label the different clusters of samples and further split the variant file into two files: the

Pando variant file and the surrounding clones variant file, with 9 424 and 20 178 SNPs, respectively.

Identifying somatic mutations. To filter out the germline mutations and only be left with the somatic mutations, we first compared each dataset (replicates, fine scale and large scale) with the surrounding clones set of variants and a 'panel of normals' and only kept the variants unique to dataset of focus. The 'panel of normals' (42) is composed of 100 samples of *P. tremuloides* from Utah neighboring states (Idaho, Wyoming, Colorado, Nevada) that were collected and sequenced with the large scale dataset in 2008. Next, we labeled samples as homozygotes or heterozygotes for every variant detected by comparing their probability of being heterozygote to the threshold value (.95). To remove variants that may have been present in the mother seed of the organism, we removed the SNPs that were found in 80% or more of the samples. We also removed the variants that were only found in one sample, as they could be either rare variants, or sequencing errors. We filtered out individuals with a mean coverage of $<4\times$ for all variants. We then performed a spatial structure analysis on the filtered sets of somatic mutations.

Spatial analyses. To detect spatial structure in the dataset, we applied the same set of analyses on two different datasets: (1) a large scale, and (2) a finer scale dataset. We first compared the proportion of shared variants per pair of samples to their physical distance (number of shared mutations between a pair of samples, divided by the mean number of mutations for the same pair of samples). We then compared the mean distance between groups of samples sharing a mutation. We used Vincenty ellipsoid method (distVincentyEllipsoid function in R) to calculate the shortest spatial distance between two samples. For each analysis, we compared the empirical values to values obtained from a randomized dataset to assess the significance of the results. To generate null distributions, we randomized either the genotypes or the pair of spatial coordinates, (latitude and longitude) and ran the same analysis as ran on the non-permuted data (500 or 1000 permutations).

Coalescent model using BEAST. We used the software package BEAST (version 2.7.5) to estimate the height of the phylogenetic tree for the Pando samples based on the accumulated somatic mutations; this was done on a coalescent Bayesian skyline model for effective population size (27, 43, 44). We chose the GTR nucleotide-substitution model to account for unequal substitutions rates between bases (45). The nexus file was obtained by concatenating the set of somatic SNPs with binary coding of the presence of the homozygote genotype with one of the base pair (for example, "A"), a heterozygote with another base pair (for example, "T") and a missing site (no variant calling information for that site) with an "N". The chains were run for 7×10^7 states. To estimate the age of the tree, we converted the phylogeny height to years *a posteriori* following this calculation:

$$\text{age(years)} = \frac{T n_S}{n_{BP}} * \frac{3}{\mu}$$

with T being the phylogenetic tree height as given by BEAST, n_S the total number of mutations, n_{BP} , the total number of base pairs sequenced, μ the leaf somatic mutation

1241 rate ($1.33 * 10^{-10}$ per base per haploid genome per year (28)),
1242 taking into account that the Pando clone is triploid (20, 29).
1243 The total number of base pairs sequenced (129,194,577)
1244 was estimated using *angsd* (46), and reduced following the
1245 proportion of base pairs that we filtered out based on coverage
1246 (48%).

1247 **Accounting for missing mutations.** We compared the number
1248 of common mutations between the replicate dataset set of
1249 somatic mutations, and mutations from the 12 samples of the
1250 finer scale, from which the replicate samples were derived. 6
1251 mutations (out of 101) were common between both datasets,
1252 implying that we are missing 96% of the somatic mutations.
1253 To take this into account as well as how the phylogenetic
1254 tree height might be affected with missing mutations, we
1255 calculated the relationship between the number of missing
1256 mutations and the phylogeny height. To do so, we randomly
1257 removed an increasing percentage of mutations, simulated the
1258 phylogeny in BEAST and found a linear relationship between
1259 the proportion of missing mutations and the phylogenetic tree
1260 height. We used this regression to estimate the Pando clone
1261 age.

1262 1. R Ekblom, J Galindo, Applications of next generation sequencing in molecular ecology of
1263 non-model organisms. *Heredity* **107**, 1–15 (2011).
1264 2. R Lanfear, Do plants have a segregated germline? *PLoS biology* **16**, e2005439 (2018).
1265 3. F Berger, D Twell, Germline specification and function in plants. *Annu. review plant biology*
1266 **62**, 461–484 (2011).
1267 4. E Bricker, A Calladine, R Virnstein, M Waycott, Mega clonality in an aquatic plant—a potential
1268 survival strategy in a changing environment. *Front. plant science* **9**, 435 (2018).
1269 5. JB Anderson, et al., Clonal evolution and genome stability in a 2500-year-old fungal individual.
1270 *Proc. Royal Soc. B* **285**, 20182233 (2018).
1271 6. GG Wang, Early regeneration and growth dynamics of *populus tremuloides* suckers in
1272 relation to fire severity. *Can. J. For. Res.* **33**, 1998–2006 (2003).
1273 7. JF Johnstone, Effects of aspen (*populus tremuloides*) sucker removal on postfire conifer
1274 regeneration in central alaska. *Can. J. For. Res.* **35**, 483–486 (2005).
1275 8. T Steinger, C Körner, B Schmid, Long-term persistence in a changing climate: Dna analysis
1276 suggests very old ages of clones of alpine *carex curvula*. *Oecologia* **105**, 94–99 (1996).
1277 9. S Tomimoto, A Satake, Modelling somatic mutation accumulation and expansion in a
1278 long-lived tree with hierarchical modular architecture. *J. Theor. Biol.* **565**, 111465 (2023).
1279 10. JM Edgelo, et al., Extensive polyploid clonality was a successful strategy for seagrass to
1280 expand into a newly submerged environment. *Proc. Royal Soc. B* **289**, 20220538 (2022).
1281 11. S Arnaud-Haond, et al., Implications of extreme life span in clonal organisms: millenary
1282 clones in meadows of the threatened seagrass *posidonia oceanica*. *PLoS one* **7**, e30454
1283 (2012).
1284 12. TB Reusch, C Boström, Widespread genetic mosaicism in the marine angiosperm *zostera*
1285 *marina* is correlated with clonal reproduction. *Evol. Ecol.* **25**, 899–913 (2011).
1286 13. L Wang, et al., The architecture of intra-organism mutation rate variation in plants. *PLoS*
1287 *biology* **17**, e3000191 (2019).
1288 14. RP Anderson, FA Macdonald, DS Jones, S McMahon, DE Briggs, Doushantuo-type
1289 microfossils from latest ediacaran phosphorites of northern mongolia. *Geology* **45**,
1079–1082 (2017).
1290 15. E Schmid-Siegert, et al., Low number of fixed somatic mutations in a long-lived oak tree. *Nat.*
1291 *Plants* **3**, 926–929 (2017).
1292 16. NV DeByle, RP Winokur, *Aspen: ecology and management in the western United States*. (US
1293 Department of Agriculture, Forest Service, Rocky Mountain Forest and ...) Vol. 119, (1985).
1294 17. J DeWoody, CA Rowe, VD Hipkins, KE Mock, "pando" lives: molecular genetic evidence of a
1295 giant aspen clone in central utah. *West. North Am. Nat.* **68**, 493–497 (2008).

1296 **Pollen analysis.** Pollen analysis followed standard acid diges-
1297 tion procedures (47). Pollen residues were classified and
1298 tabulated using light microscopy at 40x until a minimum
1299 of 300 terrestrial grains were counted. Pollen identification
1300 was assisted by relevant keys and literature (e.g., Kapp et al.
1301 2000 (48)). We assume that the *Populus* pollen type, which is
1302 generally not diagnostic to species-level assignment, reflects
1303 quaking aspen in this environmental setting.

1304 **ACKNOWLEDGMENTS.** We would like to thank the GT QBioS
1305 Graduate Program for its support and the Society for the Study
1306 of Evolution for granting a Rosemary Grant Advanced Award
1307 to Rozenne Pineau that helped with pushing this work forward.
1308 This work was initiated by a seed grant from AV and JM. The
1309 work was further supported by grants from the NIH (Grant No.
1310 5R35GM138030), the NSF Division of Environmental Biology
1311 (Grant No. DEB-1845363) to WCR and (Grant No. DEB-1844941)
1312 to ZG, and the NSF grant Paleo Perspectives on Climate Change
1313 (P2C2) Program (Grant No. 2102997) to JM and AB. The support
1314 and resources from the Center for High Performance Computing at
1315 the University of Utah are gratefully acknowledged.

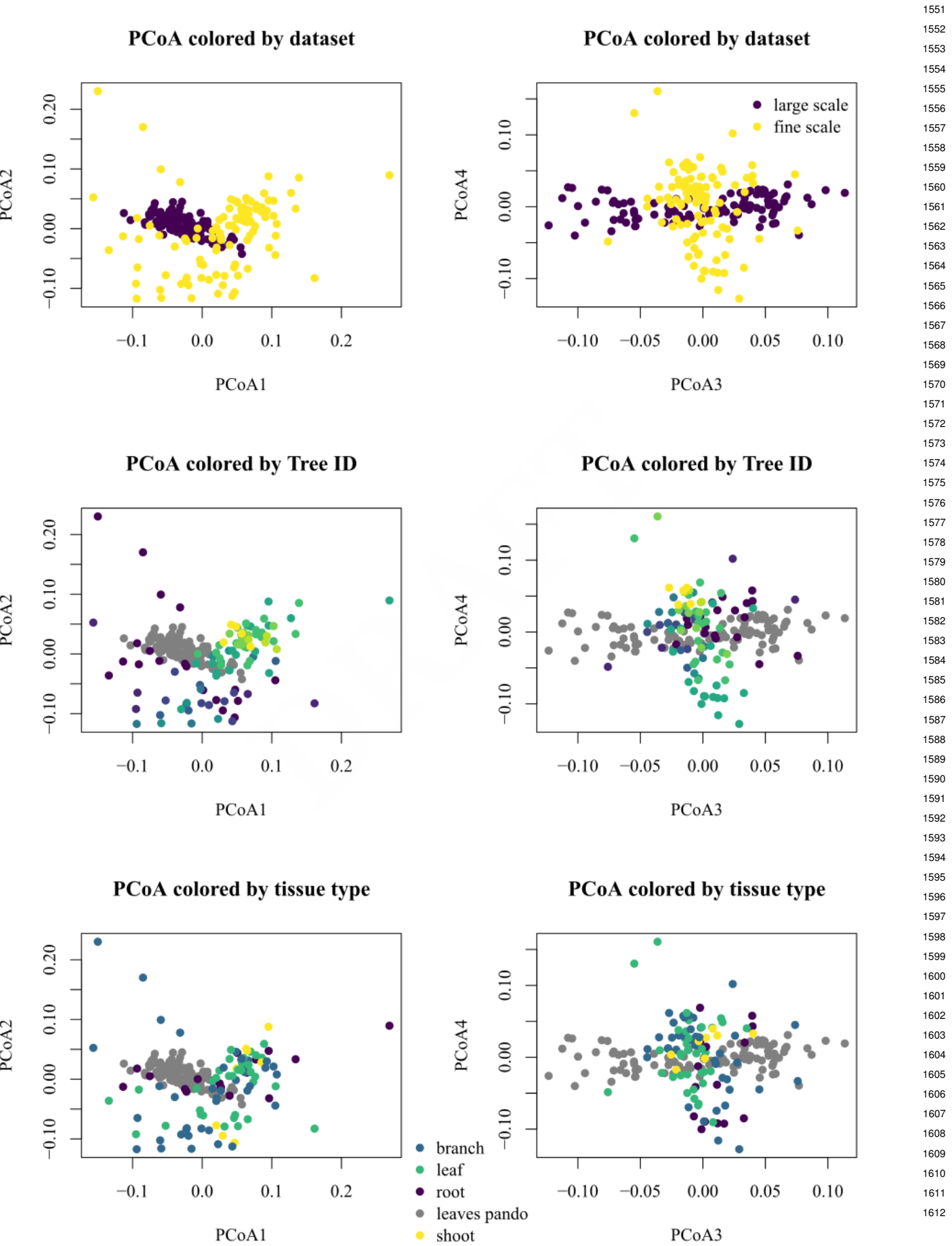
1316 18. MC Grant, The trembling giant. *Discover* **14**, 82 (1993).
1317 19. BV Barnes, The clonal growth habit of american aspens. *Ecology* **47**, 439–447 (1966).
1318 20. KE Mock, C Rowe, MB Hooten, J Dewoody, V Hipkins, Clonal dynamics in western north
1319 american aspen (*populus tremuloides*). *Mol. Ecol.* **17**, 4827–4844 (2008).
1320 21. YC Lin, et al., Functional and evolutionary genomic inferences in *populus* through genome
1321 and population sequencing of american and european aspen. *Proc. Natl. Acad. Sci.* **115**,
E10970–E10978 (2018).
1322 22. SR Narum, CA Buerkle, JW Davey, MR Miller, PA Hohenlohe, Genotyping-by-sequencing in
1323 ecological and conservation genomics. *Mol. ecology* **22**, 2841 (2013).
1324 23. I Martincovic, PJ Campbell, Somatic mutation in cancer and normal cells. *Science* **349**,
1483–1489 (2015).
1325 24. M Schirmer, R D'Amore, UZ Ijaz, N Hall, C Quince, Illumina error profiles: resolving fine-scale
1326 variation in metagenomic sequencing data. *BMC bioinformatics* **17**, 1–15 (2016).
1327 25. MW Day, The root system of aspen. *Am. Mid. Nat. pp.* 502–509 (1944).
1328 26. X Vekemans, OJ Hardy, New insights from fine-scale spatial genetic structure analyses in
1329 plant populations. *Mol. ecology* **13**, 921–935 (2004).
1330 27. AJ Drummond, A Rambaut, B Shapiro, OG Pybus, Bayesian coalescent inference of past
1331 population dynamics from molecular sequences. *Mol. biology evolution* **22**, 1185–1192
1332 (2005).
1333 28. BT Hofmeister, et al., A genome assembly and the somatic genetic and epigenetic mutation
1334 rate in a wild long-lived perennial *populus trichocarpa*. *Genome Biol.* **21**, 1–27 (2020).
1335 29. KE Mock, et al., Widespread triploidy in western north american aspen (*populus tremuloides*).
1336 *PLoS One* **7**, e48406 (2012).
1337 30. PU Clark, et al., The last glacial maximum. *science* **325**, 710–714 (2009).
1338 31. SJ Marshall, TS James, GK Clarke, North american ice sheet reconstructions at the last
1339 glacial maximum. *Quat. Sci. Rev.* **21**, 175–192 (2002).
1340 32. DW Marchetti, MS Harris, CM Bailey, TE Cerling, S Bergman, Timing of glaciation and last
1341 glacial maximum paleoclimate estimates from the fish lake plateau, utah. *Quat. Res.* **75**,
183–195 (2011).
1342 33. RJ DeRose, KE Mock, JN Long, Cytotype differences in radial increment provide novel insight
1343 into aspen reproductive ecology and stand dynamics. *Can. J. For. Res.* **45**, 1–8 (2015).
1344 34. D Ally, K Ritland, S Otto, Can clone size serve as a proxy for clone age? an exploration using
1345 microsatellite divergence in *populus tremuloides*. *Mol. Ecol.* **17**, 4897–4911 (2008).
1346 35. MK Pandit, MU Pocock, WE Kunin, Ploidy influences rarity and invasiveness in plants. *J. Ecol.*
1347 **99**, 1108–1115 (2011).
1348 36. D Ally, K Ritland, SP Otto, Aging in a long-lived clonal tree. *PLoS Biol.* **8**, e1000454 (2010).
1349 37. IJ Chybicki, M Trojankiewicz, A Oleksa, A Dzialuk, J Burczyk, Isolation-by-distance within
1350 naturally established populations of european beech (*fagus sylvatica*). *Botany* **87**, 791–798
1351 (2009).
1352 38. P Kuss, AR Pluess, HH Ægisdóttir, J Stöcklin, Spatial isolation and genetic differentiation in
1353 naturally fragmented plant populations of the swiss alps. *J. Plant Ecol.* **1**, 149–159 (2008).
1354 39. A Burian, P Barberi de Reuille, C Kuhlemeyer, Patterns of stem cell divisions contribute to
1355 plant longevity. *Curr. Biol.* **26**, 1385–1394 (2016).
1356 40. Z Gompert, et al., Admixture and the organization of genetic diversity in a butterfly species
1357 complex revealed through common and rare genetic variants. *Mol. ecology* **23**, 4555–4573
1358 (2014).
1359 41. H Li, et al., The sequence alignment/map format and samtools. *bioinformatics* **25**, 2078–2079
1360 (2009).
1361 42. Y Dou, HD Gold, LJ Luquette, PJ Park, Detecting somatic mutations in normal cells. *Trends*
1362 *Genet.* **34**, 545–557 (2018).
1363 43. R Bouckaert, et al., Beast 2: a software platform for bayesian evolutionary analysis. *PLoS*
1364 *computational biology* **10**, e1003537 (2014).

1365 44. R Bouckaert, et al., Beast 2.5: An advanced software platform for bayesian evolutionary
1366 analysis. *PLoS computational biology* **15**, e1006650 (2019). 1427
1367 45. PJ Waddell, M Steel, General time-reversible distances with unequal rates across sites:
1368 mixing γ and inverse gaussian distributions with invariant sites. *Mol. phylogenetics evolution*
1369 **8**, 398–414 (1997). 1429
1370 46. TS Korneliussen, A Albrechtsen, R Nielsen, Angsd: analysis of next generation sequencing
1371 data. *BMC bioinformatics* **15**, 1–13 (2014). 1430
1372 47. K Fagri, J Iversen, Textbook of pollen analysis (3rd version) (1989). 1432
1373 48. RO Kapp, *Guide to Pollen and Spores*. (The American Association of Stratigraphic
1374 Palynologists Foundation, College Station, Texas), 2nd edition, (2000). 1433
1375 1434
1376 1435
1377 1436
1378 1437
1379 1438
1380 1439
1381 1440
1382 1441
1383 1442
1384 1443
1385 1444
1386 1445
1387 1446
1388 1447
1389 1448
1390 1449
1391 1450
1392 1451
1393 1452
1394 1453
1395 1454
1396 1455
1397 1456
1398 1457
1399 1458
1400 1459
1401 1460
1402 1461
1403 1462
1404 1463
1405 1464
1406 1465
1407 1466
1408 1467
1409 1468
1410 1469
1411 1470
1412 1471
1413 1472
1414 1473
1415 1474
1416 1475
1417 1476
1418 1477
1419 1478
1420 1479
1421 1480
1422 1481
1423 1482
1424 1483
1425 1484
1426 1485
1427 1486
1428 1487
1429 1488

A. Supplementary Figures

1427
1428
1429
1430
1431
1432
1433
1434
1435
1436
1437
1438
1439
1440
1441
1442
1443
1444
1445
1446
1447
1448
1449
1450
1451
1452
1453
1454
1455
1456
1457
1458
1459
1460
1461
1462
1463
1464
1465
1466
1467
1468
1469
1470
1471
1472
1473
1474
1475
1476
1477
1478
1479
1480
1481
1482
1483
1484
1485
1486
1487
1488

1489
1490
1491
1492
1493
1494
1495
1496
1497
1498
1499
1500
1501
1502
1503
1504
1505
1506
1507
1508
1509
1510
1511
1512
1513
1514
1515
1516
1517
1518
1519
1520
1521
1522
1523
1524
1525
1526
1527
1528
1529
1530
1531
1532
1533
1534
1535
1536
1537
1538
1539
1540
1541
1542
1543
1544
1545
1546
1547
1548
1549
1550



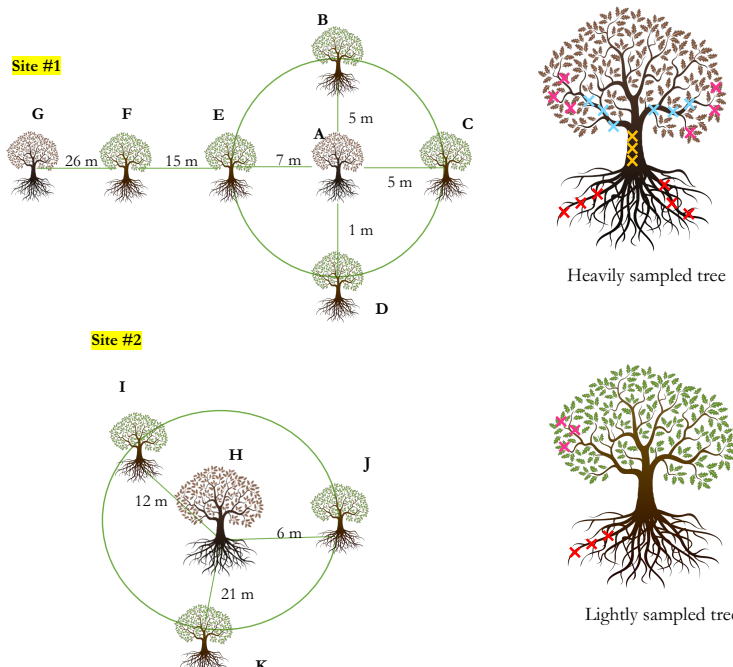
1551
1552
1553
1554
1555
1556
1557
1558
1559
1560
1561
1562
1563
1564
1565
1566
1567
1568
1569
1570
1571
1572
1573
1574
1575
1576
1577
1578
1579
1580
1581
1582
1583
1584
1585
1586
1587
1588
1589
1590
1591
1592
1593
1594
1595
1596
1597
1598
1599
1600
1601
1602
1603
1604
1605
1606
1607
1608
1609
1610
1611
1612

1613
1614
1615
1616
1617
1618
1619
1620
1621
1622
1623
1624
1625
1626
1627
1628
1629
1630
1631
1632

1675
1676
1677
1678
1679
1680
1681
1682
1683
1684
1685
1686
1687
1688
1689
1690
1691
1692
1693
1694
1695
1696
1697
1698
1699
1700
1701
1702
1703
1704
1705
1706
1707
1708
1709
1710
1711
1712
1713
1714
1715
1716
1717
1718
1719
1720
1721
1722
1723
1724
1725
1726
1727
1728
1729
1730
1731
1732
1733
1734
1735
1736



Fig. A.2. Localities for large scale (left) and fine scale (right) sampling. Coordinates are given in Supplementary Table 1.



- ✗ Roots: 3 samples along one root, two roots
- ✗ Shoot: 3 samples along the shoot
- ✗ Branch: 3 samples along the branch, two branches
- ✗ Leaves: 3 samples from the same branch, two branches

Fig. A.3. Sampling strategy for the fine scale dataset. Leaf, bark, branch and root samples from two localities within the Pando stand were collected. In site #1, located in a recently clear cut area, two ramets were heavily sampled (leaf, bark, branch and root samples), and five surrounding ramets were lightly sampled (leaf and root samples). In site #2, one ramet was heavily sampled and three surrounding ramets were lightly sampled.

1737

1738

1739

1740

1741

1742

1743

1744

1745

1746

1747

1748

1749

1750

1751

1752

1753

1754

1755

1756

1757

1758

1759

1760

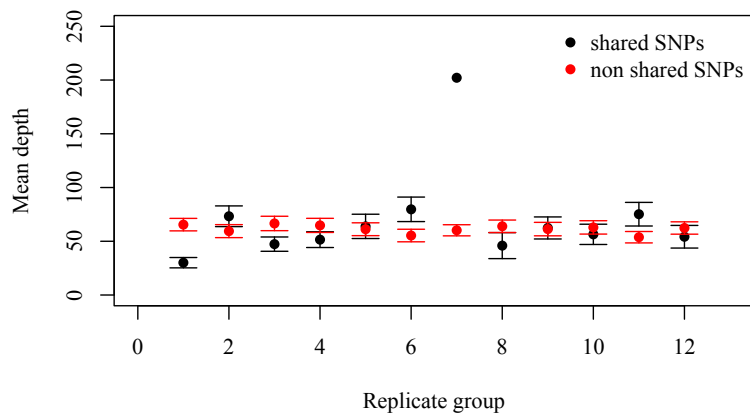


Fig. A.4. The mean read depth per SNP for the mutations that were found in more than 2 sample per replicate group was not different from the mean read depth of the mutations that were not found in more than 2 samples per group (two-sided Student's test, $t = 0.69$, $P = 0.51$). Error bars indicate standard error. Replicate group 7 only had 2 samples left after filtering and was removed from downstream analyses.

1761

1762

1763

1764

1765

1766

1767

1768

1769

1770

1771

1772

1773

1774

1775

1776

1777

1778

1779

1780

1781

1782

1783

1784

1785

1786

1787

1788

1789

1790

1791

1792

1793

1794

1795

1796

1797

1798

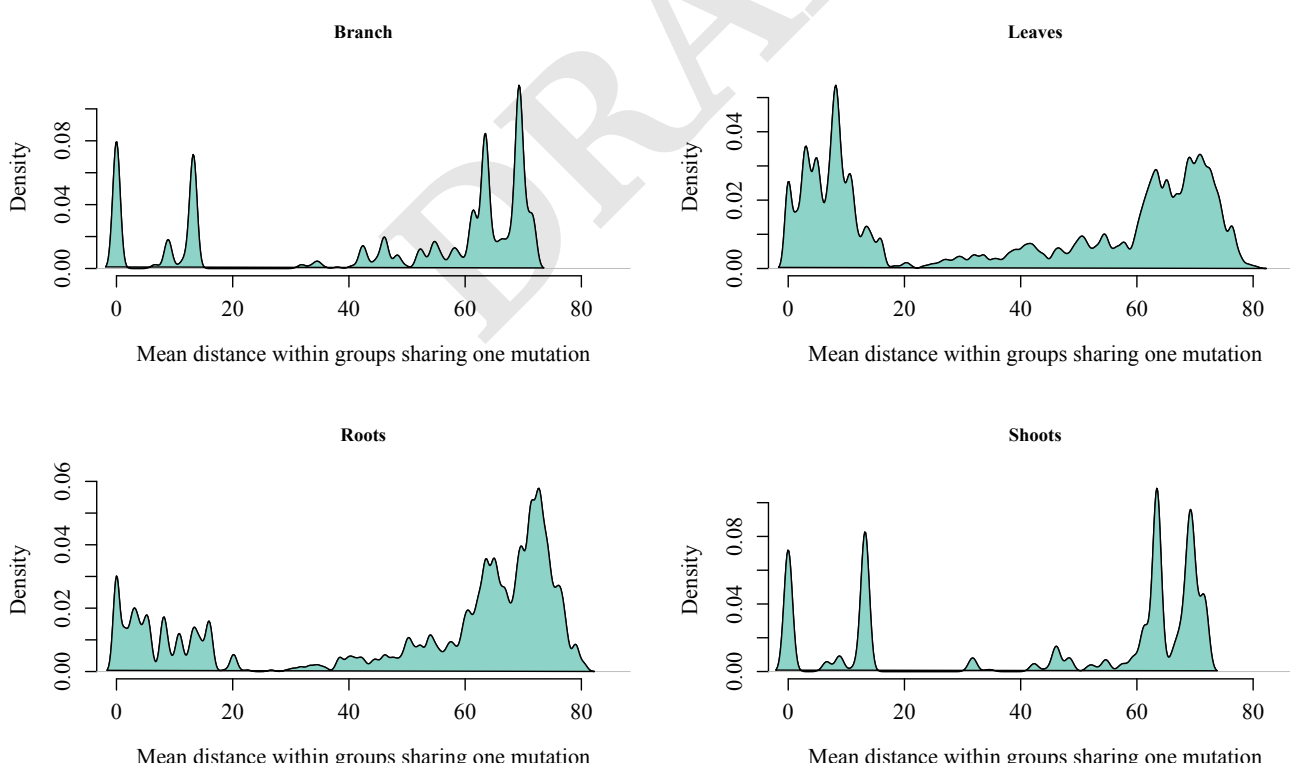


Fig. A.5. Distributions of mean correlations between the spatial distance between pairs of samples, and the number of mutations they have in common, sorted by tissue type. Correlation value for root is -0.11 , correlation value for leaves is -0.44 , correlation value for shoots is -0.05 , correlation for branch is -0.06 .

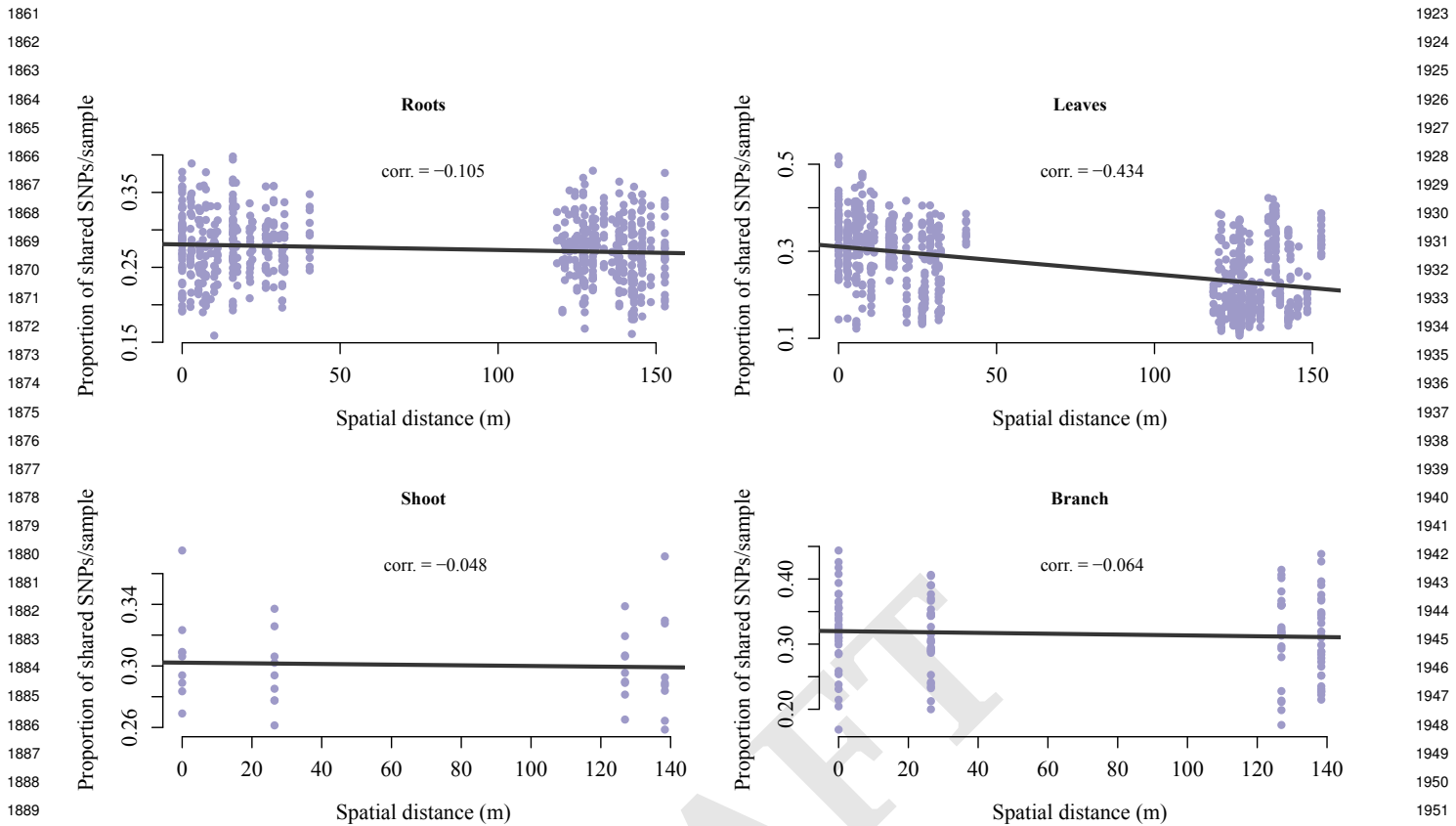


Fig. A.6. Distributions of mean distance between samples sharing one mutation in the fine scale dataset, sorted by tissue type. Mean distance for leaves is 39.28 m, mean distance for roots is 51.36 m, mean distance for shoots is 46.12 m, mean distance for branches is 46.69 m.

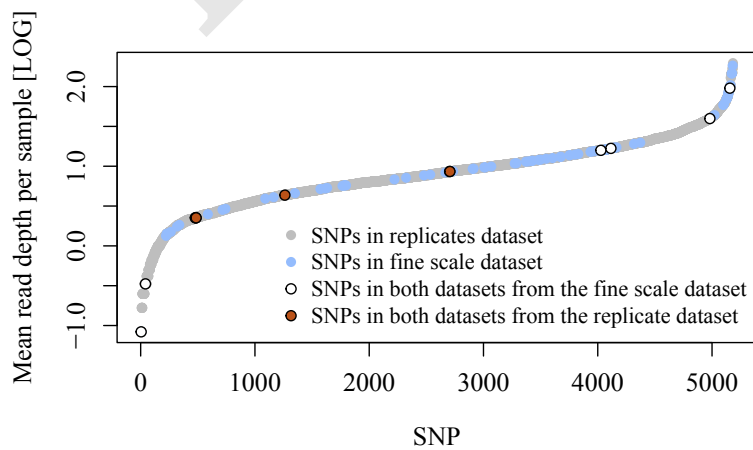


Fig. A.7. The mean read depth per sample is overall higher in the "replicates" dataset (gray) than in the "fine-scale" dataset (blue). However some mutations found in both datasets (the "replicates" and "fine-scale" datasets, in orange and white, respectively) had coverage as low as 6x in the "fine scale" dataset.

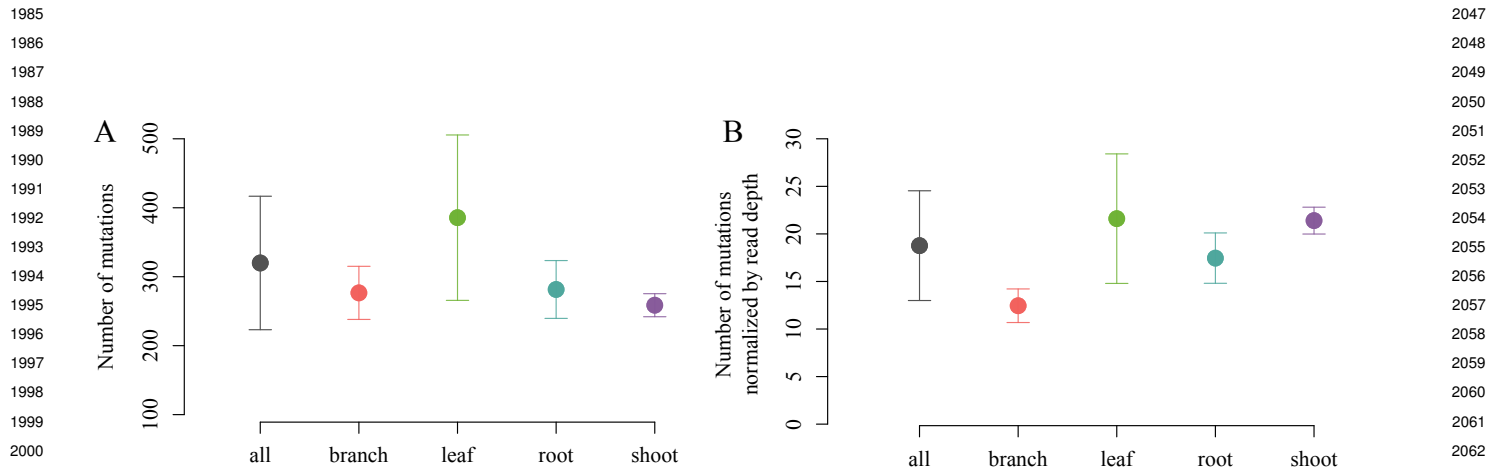


Fig. A.8. (A) The number of somatic mutations differs between tissue types (ANOVA, $F_{3,97} = 14.47$, $P = 7.26e^{-8}$), with the leaves having a significantly higher number of mutations as compared to the roots, branches or the shoot (Tukey HSD's $P < 0.0003$). (B) When normalized by read depth, the leaves still show a significantly higher number of mutations as compared to root and branches, but not shoot (ANOVA, $F_{3,97} = 16.55$, $P = 9.22e^{-9}$ followed by Tukey HSD with $P < 0.0001$ for root and branch).

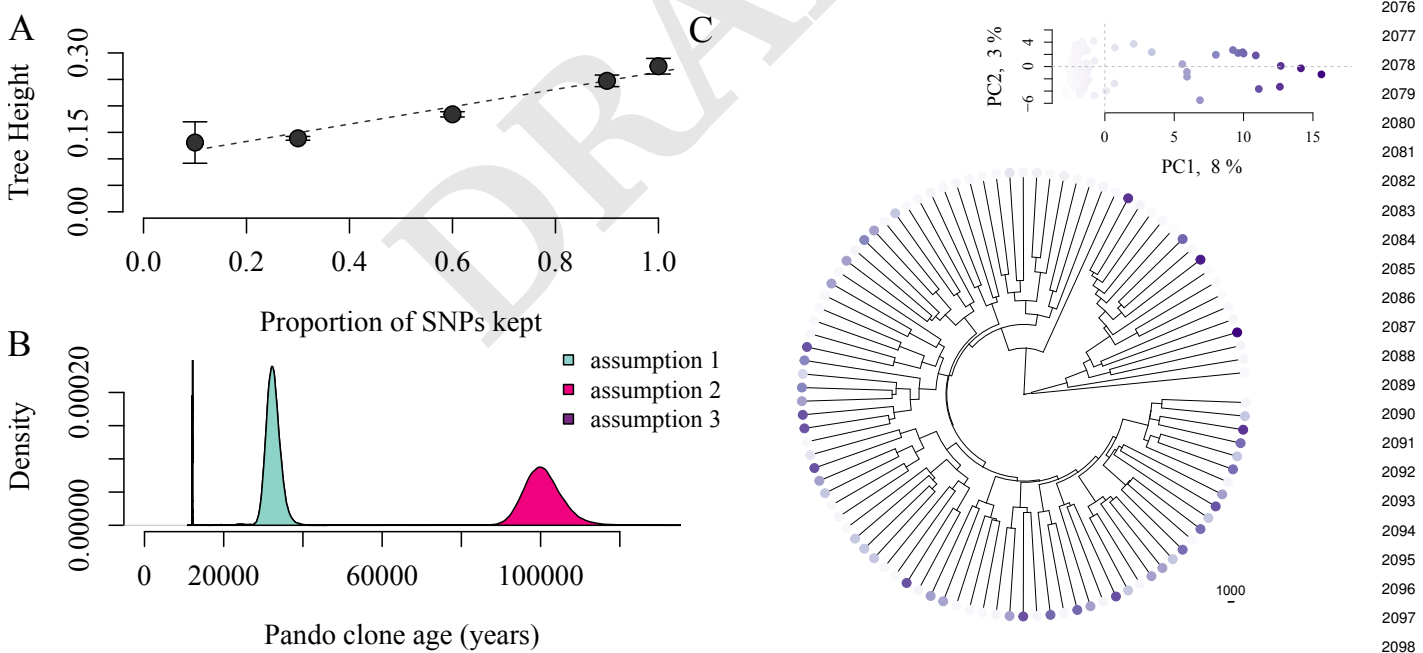


Fig. A.9. The Pando clone is more than 100 000 years old based on the fine scale dataset. (A) We use the relationship between the proportion of missing mutations from a simulated dataset and the phylogenetic tree height to take into account the somatic mutations that we are missing in the Pando clone fine scale dataset (linear regression $y = 0.10 + 0.16x$, $P < 2.2e-16$, $R^2 = 0.82$). (B) With this correction, we calculate the Pando clone age based on three different assumptions: (1) if the mutations we detect are all real, the Pando clone would be about 32 423 years old ($\pm sd = 2154$ years); (2) if we are missing 94% of the mutations, then the clone would on average be 100375 years old ($\pm sd = 5882$ years); (3) finally, if only 6% of the mutations we detect are real somatic mutations, the Pando clone would be 12145 years old ($\pm sd = 21$ years). (C) Despite thousands of years of evolutionary history, the Pando clone shows minimal phylogenetic structure (points colored according to PC1 score).